Effects of Filler Wire Intervention on the Gas Tungsten Arc: Part III — Process Stability Control of Wire-Filled GTAW

A sensing method that collects global and local arc information was used to monitor the stability of metal transfer and weld surface height

BY S. ZOU, Z. WANG, Y. CAO, AND S. HU

Abstract

Stability control of the welding process is necessary to guarantee weld quality. In this study, a sensing method that collects both global and local arc information was proposed to conveniently monitor metal transfer stability during gas tungsten arc welding. This sensing method was also used to monitor the stability of the weld surface height by sensing the change in global arc length. The stability factor (f_{mt}) was calculated to quantify the metal transfer stability. The characteristic signal (U^*), which represents the average global arc voltage in the presence of a liquid bridge, was extracted to characterize the change in arc length by decoupling the dynamic interference signal of metal transfer. Both a fuzzy controller and a proportional integral derivative controller were designed to control the metal transfer stability and the weld surface height. The preliminary control experiments proved the effectiveness and potential of the proposed sensing and control strategies.

Keywords

- Metal Transfer
- Process Stability
- Arc Voltage
- Arc Sensing
- Feedback Control
- Wire-Filled Gas Tungsten Arc Welding (GTAW)

Introduction

Automated gas tungsten arc welding (GTAW) has matured into a well-established manufacturing technique that is frequently used in aerospace, nuclear power, etc. Its process stability has long been one of the main concerns in the welding community (Ref. 1). For GTAW in complex environments, real-time assurance of the stability of the weld surface height and metal transfer is of great significance to the quality of weld shaping. Real-time monitoring for these purposes often requires the establishment of process sensing and control systems; therefore, this work proposed a practical arc sensing method to achieve real-time feedback control of the weld surface height and metal transfer in GTAW.

In general, the process stability of GTAW partly depends on the stability of the weld surface height. This height will vary for many reasons, such as alignment/fitup errors, welding torch movement or positioning errors, the accumulated unevenness from the previous pass, etc. An unduly convex weld surface is likely to cause short-circuiting contact and tungsten inclusion when the filler metal is added. Additionally, if the weld surface is too far from the tungsten electrode, the arc stability will be weakened, and this surface will also face insufficient gas shielding. The uneven height of the weld surface will increase the risk of weld defects and may impact subsequent welding. Thus, it makes sense to monitor the change in this height.

A direct monitoring method has been used to capture images of the weld surface height. This method involves mounting a camera with optical filters (i.e., passive vision sensing), where the distance from the tip of the nonconsumable tungsten electrode to the weld surface can be extracted by image processing to characterize the variation in the weld surface height (Refs. 2–4). A mirror imaging method has
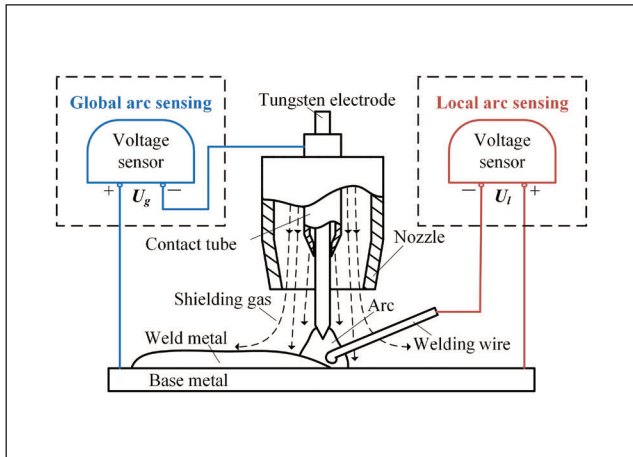
Fig. 1 — Schematic diagram of the global and local arc sensing method.

also been proposed to capture the reversed reflection of the tungsten electrode under an appropriate exposure (Refs. 5, 6). This method used the mathematical specular reflection model to obtain the distance between the tungsten electrode tip and its reversed image, which was used as a variable to estimate the weld pool surface height. Another vision-based method that has received much attention involves active structured-light vision sensing, which can monitor the dynamic evolution of the surface height by processing the two-dimensional structured-light reflection images (Refs. 7, 8) or by reconstructing the three-dimensional (3D) weld pool (Refs. 9–12). Based on the reconstructed 3D coordinates of the weld pool surface, Zhang et al. (Ref. 13) as well as Liu and Zhang (Ref. 14) extracted several geometrical parameters — such as the weld surface convexity (i.e., average height of the weld pool), length, and width — to estimate the backside bead geometry. Liu and Zhang (Ref. 15) also realized the predictive control of the weld pool surface by establishing a linear model between the weld surface convexity, length, and width and the welding current and speed. In another study (Ref. 16), the empirical response of the human welder to the real-time state of the topside weld pool was modeled as a neuro-fuzzy inference system, which was used for the feedback control of the weld pool geometry. There are more nonvisual sensing methods available, including arc acoustic sensing (Refs. 17–19) and arc light sensing (Refs. 20, 21). These two methods can assess the surface height by acoustoelectric or photoelectric measurement of the arc length. All of the aforementioned are noncontact sensing methods, which means that a sensing system independent of the welding circuit needs to be established. As a result, limitations can arise when spatial accessibility, welding posture, and so forth are taken into account.

The arc sensing method, which takes the welding arc itself as a sensor to extract electrical signals directly from the welding circuit without the demand for complex external systems, is easier to implement and more cost-effective in engineering applications. Based on the inherent relationship between arc voltage and arc length in GTAW (Ref. 22), this method has been applied in weld joint penetration control (Refs. 23, 24) and automatic voltage control (AVC) (Refs.

25, 26). Although it is generally believed that the change in the weld surface height can be characterized by arc voltage due to the change in arc length caused by its change, using the arc voltage to characterize the change in the weld surface height or arc length still has its limitations because the arc voltage is also affected by the electrical noise, dynamic behaviors of the liquid filler metal (if filler metal is added), etc. The filter is usually designed to filter out the high-frequency noise in the arc voltage (Ref. 27) so that arc sensing remains relatively reliable during autogenous GTAW.

However, in wire-filled GTAW, the dynamic behaviors of the liquid filler metal will affect the welding arc, and the resultant nonhigh-frequency signal components will be coupled into the arc voltage (Refs. 28, 29). This coupling makes it difficult to remove the nonhigh-frequency signal components by filtering, thus reducing the monitoring accuracy of the weld surface height or arc length by arc sensing. Additionally, the molten metal at the end of the filler wire (herein referred to as welding wire) is always expected to transfer smoothly into the weld pool so as to minimize the oscillation, spatter, or burning loss caused by its interaction with the welding arc, whereas metal transfer stability is sometimes difficult to guarantee in complex conditions (e.g., variable welding posture, narrow space, or high deposition rate). Furthermore, there are relatively few convenient methods for monitoring and characterizing metal transfer stability.

The following raises two issues about the process stability monitoring of wire-filled GTAW. One is how to conveniently monitor the metal transfer and the other is how to better monitor the change in the weld surface height or arc length under the interference of metal transfer based on arc sensing. To address the two issues, this work proposed a global and local arc sensing method, and two related characteristic signals were extracted and analyzed. Based on this method, additional welding experiments were conducted to present the results of a feasibility study on controlling the metal transfer stability and the weld surface height.

Arc Sensing and Metal Transfer

The conventional arc sensing method usually only measures the arc voltage between the base metal and tungsten electrode, which includes the global voltage drop between the cathode and anode of the welding arc. In this work, this method was extended to a dual-path arc sensing method in which the global arc voltage between the base metal and tungsten electrode (denoted as U_g) as well as the local arc voltage between the base metal and welding wire (denoted as U_l) were measured simultaneously. For brevity and convenience of description, the sensing for U_g and U_l is referred to herein as global arc sensing and local arc sensing, respectively. Figure 1 presents a schematic diagram of the arc sensing method, in the direct-current welding mode, proposed in this work.

When a current flows through the welding circuit, the measured arc voltage depends on the length and electrical characteristics of the measured arc. In global arc sensing, the weld surface height changes U_g by affecting the arc length, while the intervention of the welding wire affects U_g by changing the arc characteristics (Refs. 28, 29). The influence of
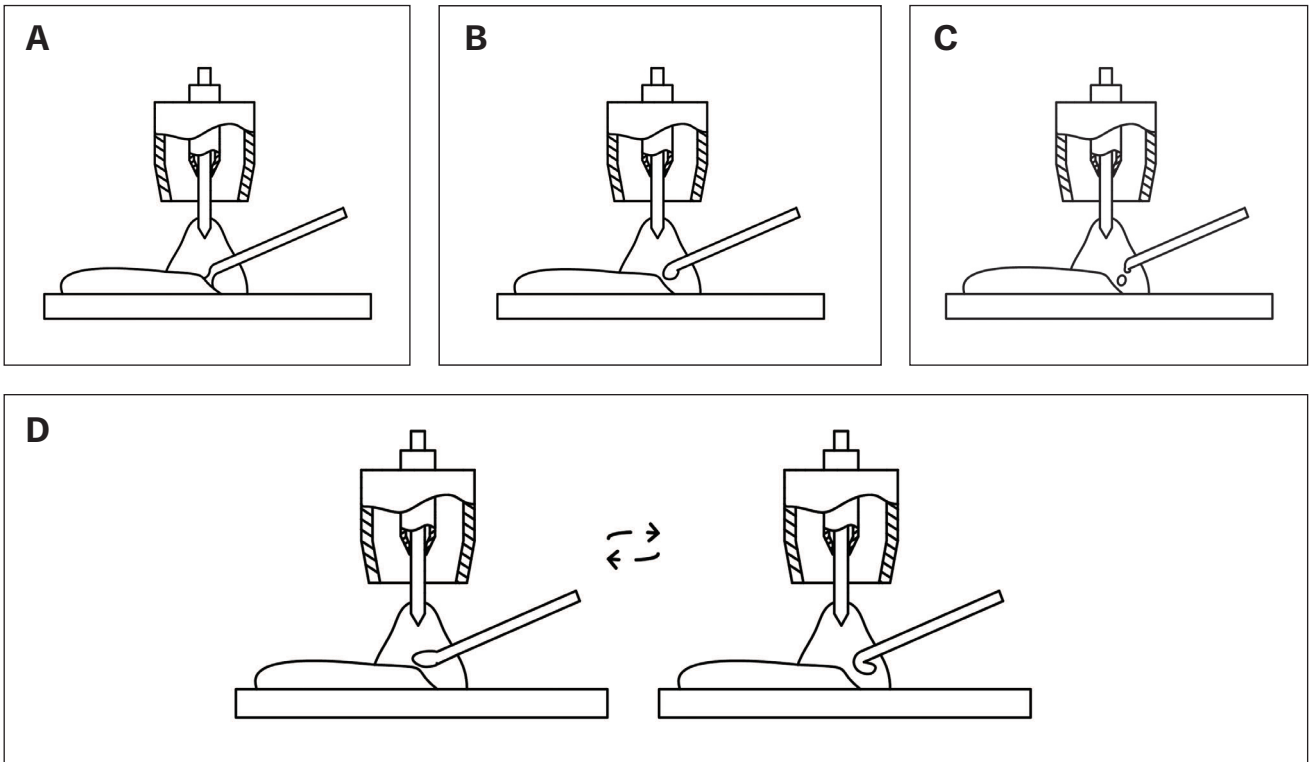
Fig. 2 — The possible states of the liquid metal/droplet: A — Bridging state; B — growing state; C — free-flight detachment state; D — oscillation state.

the welding wire on U_g is usually not static because the liquid metal droplet generated at its end may completely or partially go through a transition process (including growth, oscillation, detachment, and transfer to the weld pool) that will affect the arc characteristics to varying degrees. In addition, the influence of the weld surface height and metal transfer on U_g is superimposed, so it is difficult to distinguish them with a single U_g. This superimposition indicates the necessity of mining other sensing data.

In local arc sensing, the consumable welding wire is used as a measuring terminal to measure the arc voltage in the local area of the arc, and the metal droplet exactly hangs on this consumable measuring terminal. Generally speaking, the metal transfer modes in GTAW can be categorized as uninterrupted bridging transfer, interrupted bridging transfer, and free-flight transfer. Figure 2 presents the possible states of the molten metal/droplet at the end of the welding wire at a given moment.

If the molten metal at the end of the welding wire is always in contact with the weld pool, as shown in Fig. 2A, in a given period of time, it is considered to be in the uninterrupted bridging transfer mode. Since the liquid bridge is always existent during this time, it can be inferred that U_l will always tend to zero. If the state of the molten metal alternates between what is shown in Fig. 2A and B in a given period of time, it can be classified to be in the interrupted bridging transfer mode. In this mode, U_l will change periodically between a near-zero value range and a higher nonzero value range because the liquid bridge break will cause a significant arc voltage drop between the two local arc sensing measuring terminals. Additionally, if the liquid bridge never appears

during metal transfer in a given period of time, it is considered to be in the free-flight transfer mode, as presented in Fig. 2C. In this mode, U_l will vary in a nonzero value range, and when the liquid droplet with a volume detaches from the welding wire, U_l will increase rapidly because the detachment causes the welding wire to be far from the weld pool. In addition, as shown in Fig. 2D, the pendent metal droplet at the end of the welding wire will oscillate due to internal and external forces as its volume increases, resulting in different degrees of U_l fluctuation.

The aforementioned analyzed theoretical change process of U_l from bridging transfer to free-flight transfer is shown schematically in Fig. 3. Broadly speaking, it kept at a long-term near-zero value range; began to produce a positive pulse; presented a waveform similar to a square wave; generated an apparent fluctuation with a negative pulse; and, finally, fluctuated at a nonzero value range without any pulse. The whole process corresponds to the change of the metal transfer process from stable to unstable, and in this change, the existing time of the liquid bridge became shorter and shorter, and the droplet oscillation became more and more apparent. In short, the metal transfer process was expected to be reflected in the measured U_l to some extent.

Experimental Design

Based on the proposed sensing method, the experimental system was established. The welding system of this work mainly consisted of a Fronius MagicWave 4000 GTAW power supply that worked in the constant-current mode, a GTAW
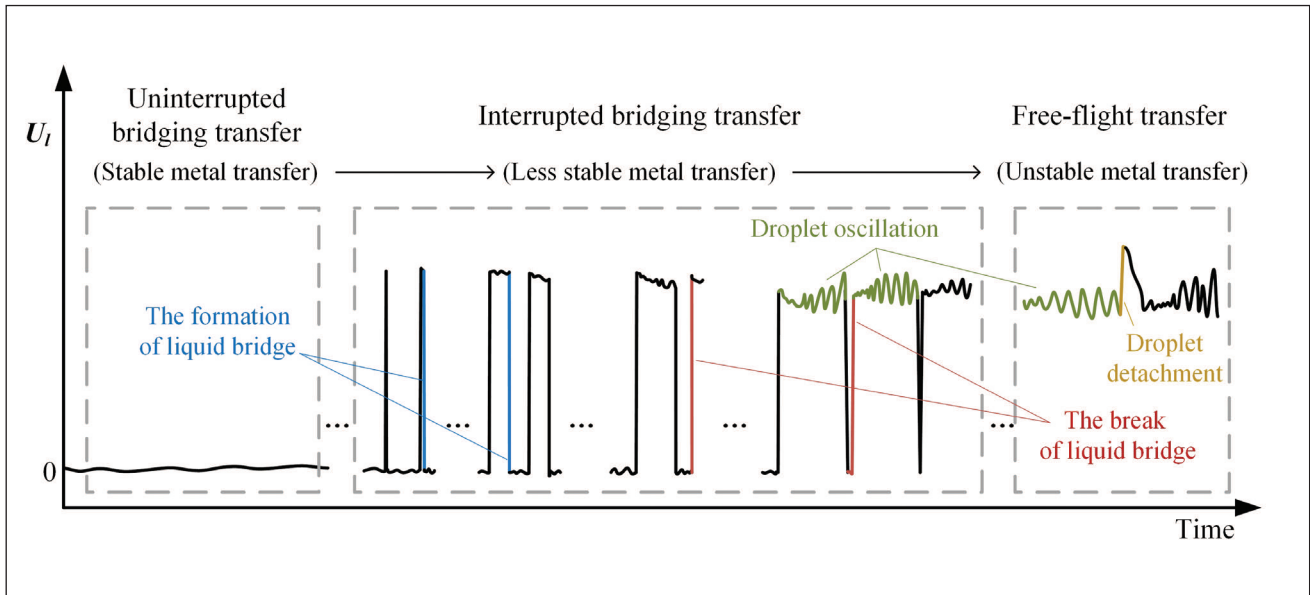
Fig. 3 — Schematic image of a typical change trend in local arc voltage U_l under different metal transfer modes.

torch, and a workpiece as the base metal. The sensing system was mainly composed of a computer, a USB-4711A data acquisition card, a Hall current sensor (used to determine that the voltage change was not caused by the current fluctuation), and two Hall voltage sensors. The signal processing and feedback controllers were realized by MATLAB® programming. The original sampling frequency of the electrical signals was 1024 Hz, at which the detailed information of metal transfer was obtained. The collected electrical signal data was filtered by a twelfth-order Butterworth low-pass filter with a passband frequency of 100 Hz, a cutoff frequency of 150 Hz, and a 40-dB attenuation. The experimental materials mainly included 4-mm-thick Q235B mild steel plates, an AWS ER70S-6 welding wire with a diameter of 1.2 mm, shielding gas of pure argon (99.99%), etc. Bead-on-plate welding experiments were conducted with the welding torch moving and the workpiece staying stationary.

Table 1 shows the overall arrangements of these welding experiments. Experiment A1 was mainly used to explain the feature extraction of arc voltage signals. Experiments B1 to B3 were used for signal analysis. Experiments C1 and C2 were aimed at the control of metal transfer. Experiments D1 to D4 plus Experiments E1 and E2 were designed for the control of the arc voltage and weld surface height, respectively. In some of the designed experiments, the height of the welding torch was adjusted to change the electrode-to-workpiece distance (ETWD) gradually (e.g., A1, C1) or quickly (e.g., step change in C2). In some other experiments, to analyze the signal changes during welding or verify the effectiveness of the feedback control, a concave pit or surface step was preset on the workpiece (e.g., B1 to B3, E1 to E2) to purposely alter the workpiece surface height.

Feature Extraction and Analysis

Signal Extraction

Figure 4 shows the arc voltage data collected under the gradual change in the ETWD in Experiment A1. Due to the inherent relationship between the arc length and arc voltage, the measured global arc voltage U_g first increased and then decreased gradually as the welding torch height changed. With the increase in ETWD, the overall fluctuation amplitude of U_g became significantly larger, a result that mainly stemmed from the influence of metal transfer. Meanwhile, the liquid bridge formed and broke with varying frequency, which caused the measured local arc voltage U_l to fluctuate violently and switch back and forth between a high value range and a low value range. It can be seen from the partial enlarged view that at the moment when the liquid bridge formed or broke, the change in U_l was as large as 4 to 5 V, far exceeding the change in U_g. This information was useful to determine whether the liquid bridge exists at a sampling moment.

If the liquid bridge existed for a longer time, the metal transfer mode was more inclined to be an uninterrupted bridging transfer (i.e., the metal transfer tended to be stable). If the liquid bridge existed for a shorter time or even zero, the interrupted bridging transfer or even the free-flight transfer accompanied by pendent droplets with a large volume was more likely to occur (i.e., the metal transfer developed toward instability). Thus, the metal transfer stability in a period of time could be quantified by the ratio of the time when the liquid bridge was absent to this period of time. This ratio was defined as the stability factor of metal transfer (denoted as f_{mt}) herein, and its expression is as follows:
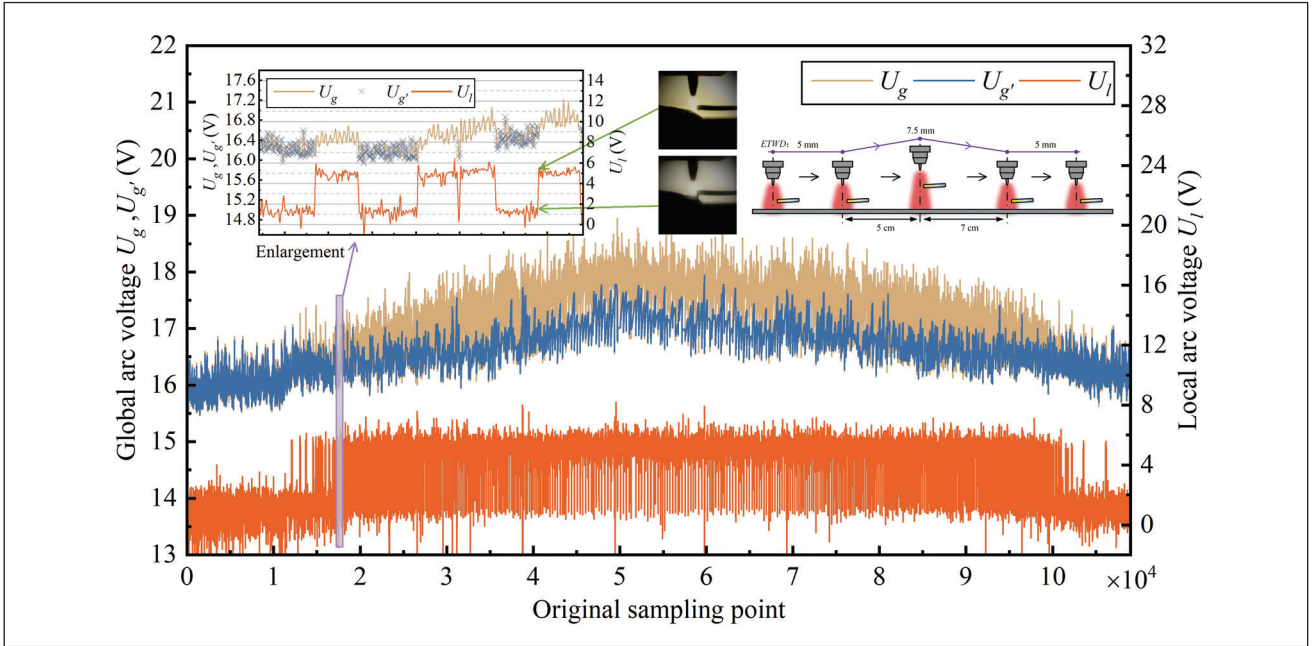
Fig. 4 — Arc voltage signals measured in Experiment A1.

$$f_{mt} = k/N \qquad (1)$$

where N is the length of the sampling window, and k is the total number of sampling points collected when the liquid bridge did not exist in this sampling window. Because of the impedance in the welding circuit, when the liquid bridge existed, U_l was actually not equal to zero, and a threshold was set to 2.9 V to represent that the liquid bridge was considered to form between the welding wire and molten pool if U_l was less than 2.9 V. The comparison between U_l and the threshold could be conducted in the sampling window, and the total number of U_l larger than the threshold, which was the value of k, was obtained. In this way, the calculated f_{mt} was between 0 and 1.

To characterize the change in arc length more accurately, it was necessary to decouple the dynamic interference of the metal transfer on U_g as far as possible. Since the specific moments when the liquid bridge existed could be obtained by the threshold judgment of U_l, the arc length could be characterized by using U_g collected only at these moments (denoted as $U_{g'}$). As can be seen in Fig. 4, compared to U_g, the signal fluctuation generated with the gradual increase in ETWD was significantly suppressed in $U_{g'}$. This way of removing the signal interference from U_g is different than some other filtering methods in that the latter are likely to only smooth the interference signal components related to the unstable metal transfer instead of decoupling them. $U_{g'}$ could be further smoothed afterwards. If all of the $U_{g'}$ collected in the sampling window of length N are expressed as $[U_{g'}(1), U_{g'}(2), …, U_{g'}(N-k)]$, the arithmetic mean can be obtained as follows:

$$U^* = [U_{g'}(1) + U_{g'}(2) +… U_{g'}(N-k)]/(N-k) \qquad (2)$$

U^* can then be used for the characterization of arc length.

The schematic diagram of signal extraction is shown in Fig. 5. Herein, N was set as 256, so the stability factor f_{mt} and arc voltage U^* were calculated every 0.25 s. Figure 6 shows the f_{mt} and U^* extracted from the arc voltage data measured in Experiment A1. The distribution of f_{mt} was in line with the actual change of metal transfer. The closer f_{mt} was to zero, the more stable the metal transfer became. Due to the shaking of the welding torch at some moments and the deformation of the workpiece in this experiment, U^* did not change strictly with the change in the nominal ETWD.
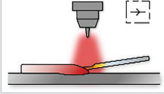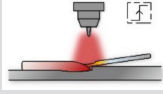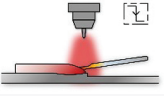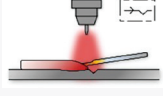
Signal Analysis

Figure 7 shows the arc voltage U^* collected in Experiments B1 and B2. In these two experiments, the welding arc was purposely extinguished before its center had crossed the preset step on the workpiece surface, and the arc crater was formed just before this step. Although the weld surface height was relatively consistent, U^* had still shown an upward trend before the arc extinction in Experiment B1 and a downward trend before the arc extinction in Experiment B2. Since the welding arc was bell shaped and its anode was an area rather than a point, U^* was not only affected by the weld pool surface height directly below the tungsten electrode but also by the surface height of the entire anode enveloped by the welding arc. Before the arc center crossed the step area, since this area had been enveloped by the arc, U^* produced a change.

Figure 8 presents the arc voltage U^* in Experiment B3. Similarly, due to the preset pit on the welding path, if the arc was extinguished when the weld pool was about to cross the pit, U^* also showed an upward trend. After the arc crossed the pit, U^* dropped and became relatively flat. The change in workpiece surface height produced a new flow in the weld pool.

Table 1 — Welding Experiment Design and Parameters

Experiment No.	Welding Current I (A)	Welding Speed v (cm · min^{-1})	Wire Feed Speed v_f (cm · min^{-1})	ETWD* (mm)	Gas Flow Rate Q (L · min^{-1})	Remarks
A1	155	7	140	[5, 7.5]	12	Gradual change in the ETWD
B1	165	10	180	5.5, 6.5	12	Preset a surface step
B2	165	10	180	6.5, 5.5	12	Preset a surface step
B3	160	10	150	5.5	12	Preset a surface pit
C1	155	7	—	[5.5, 7.5]	12	Gradual change in the ETWD
C2	165	7	—	6, 7	12	Step change in the ETWD

Experiment No.	Welding Current I (A)	Welding Speed v (cm · min^{-1})	Reference Arc Voltage U_r (V)	ETWD (mm)	Gas Flow Rate Q (L · min^{-1})	Remarks
D1	170	8	17.4	6.5	10	—
D2	170	8	17.2	6.5	10	—
D3	170	8	17.3, 17.1	6.5	10	Negative step of U_r
D4	170	8	17.2, 17.5	6.5	10	Positive step of U_r
E1	170	8	17.3	—	10	Preset a surface step
E2	170	8	17.1	—	10	Preset a surface pit

Table 1 — (continued)

Experiment No.	Design of Welding Workpiece	Experiment No.	Design of Welding Workpiece
A1, C1, C2, D1, D2, D3, D4		B2	
B1, E1		B3, E2	

*ETWD: Electrode-to-workpiece distance.

Table 2 — Fuzzy Control Rules*

Output Variable: *CV*		Input Variable: *CE*				
		PL	*PS*	*Z*	*NS*	*NL*
	PL	PL	PL	PL	PM	PM
Input Variable: *E*	PS	PL	PM	PM	PM	PS
	Z	PM	PS	NS	PS	PM

*e.g., if *E* is *PL* and *CE* is *PL*, then *CV* is *PL*.

As shown in Fig. 9, when the weld pool was close to the pit, the liquid metal at the front of the weld pool flowed downward due to gravity and filled the pit, and the liquid metal at the tail of the weld pool flowed to the front, thereby reducing the weld pool surface height. As the arc moved forward and the weld pool gradually solidified, it was difficult for the tail of the weld pool to be refilled by liquid filler metal, so the solidified weld could not maintain a stable height. Since the pit on the welding path affected the flow of the weld pool in Experiment B3, the influence of it on the weld surface height was not limited to the exact location of the pit but was extended to the nearby area and can be confirmed by the longitudinal weld section in Fig. 9. In addition, because the arc moved along the welding path at a welding speed

and gradually enveloped the area in front of it, the change in U^* did not strictly reflect the actual height change in the workpiece surface in front of the weld pool.

Control Strategies

To demonstrate the practicability of the extracted characteristic signals f_{mt} and U^*, these two signals were used as controlled variables for the feedback control of metal transfer stability and arc length (or the weld surface height), respectively.

According to the description in the previous section, the f_{mt} measured during actual welding was not negative, and for the sake of ensuring the metal transfer stability, f_{mt} was
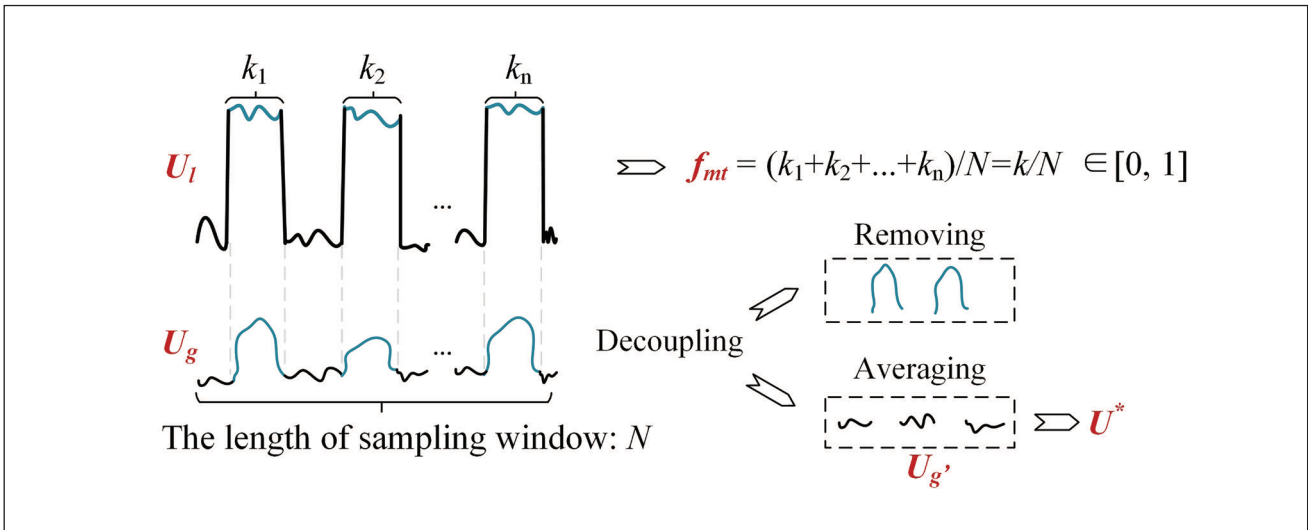
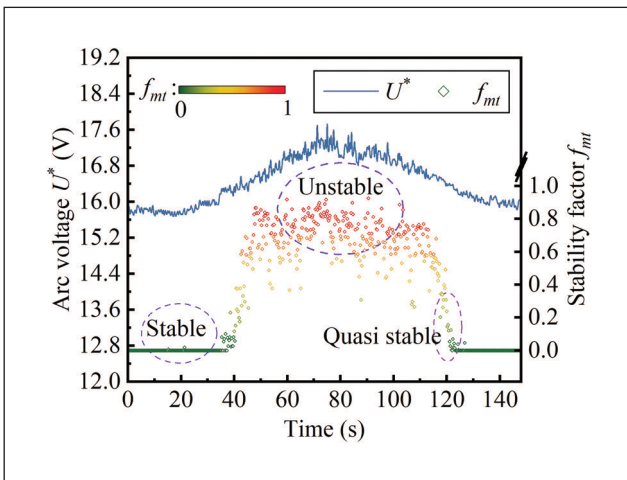*Fig. 5 — Schematic diagram of the signal extraction.*

Fig. 6 — Stability factor f_{mt} and arc voltage U^* extracted from the voltage signals in Experiment A1.

theoretically expected to remain at a value of zero. Then, the deviation of the measured value of f_{mt} from its expected value was actually equal to this nonnegative measured value, and the expected value of the deviation was also equal to zero. In view of this, if the objective of the real-time control was only to make the actual deviation tend to zero, then the control process was actually a unilateral process (i.e., the deviation only approached zero from a nonnegative value instead of a negative value). However, in the actual welding process, the case where f_{mt} is zero still needed to be further considered.

In this case, the welding wire could be melted in the welding arc, but it could also be melted directly in the weld pool, and the f_{mt} that is always zero will not provide any information about the wire feed speed being too high or the height of the welding torch being too low. If the welding wire was thus excessively fed into the weld pool, or even directly contacted the solid base metal under the weld pool, the welding process stability would be negatively affected. In this regard, adjustments, such as raising the welding torch or reducing the wire feed speed, were made so that the welding wire did

not insert too much into the weld pool (it was preferable that a liquid bridge formed between the end of the welding wire and weld pool).

Thus, a control strategy was formulated that depended on f_{mt}: If f_{mt} is positive, control its deviation to zero; if f_{mt} is zero, control the welding wire not to feed excessively. It can be seen that this control strategy was not complex, and it was not completely closed loop but partly based on subjective, empirical decision-making, which can be easily realized by fuzzy control. Using fuzzy control, after gaining a good understanding of how to control the welding process stability, the resultant empirical or intuitive decision-making can be conveniently transformed into customized rules and then directly loaded into the fuzzy controller so as to flexibly meet the control requirements in this work.

The AVC method has commercial applications in the field of GTAW and is usually used to maintain the stability of arc length. Based on the reliable linear relationship between the arc length and arc voltage within a specific range, in common commercial solutions, this method usually only needs to specify a reference value of the arc voltage and then make appropriate adjustments to indirectly realize the control of the arc length according to the deviation between the measured voltage and the reference voltage. This is done instead of presetting a value of the arc length before welding and then directly controlling the arc length to this preset value, so it is not necessary to identify the mathematical model between arc length and arc voltage.

In fact, in engineering applications, it is not easy to identify an arc length prediction model suitable for real-time control and then directly control the arc length to the preset value based on such a model. This is because it doesn't only need to consider the dynamic relationship between the arc voltage and the welding current. It also needs to consider the applicability of this model in complex welding conditions, such as changing welding postures and angles, and the arc voltage itself has limited resolution for arc length variations within a few millimeters. As a result, the control for U^* in this work followed the same strategy, and the wire feed speed v_f was selected as the adjustment parameter
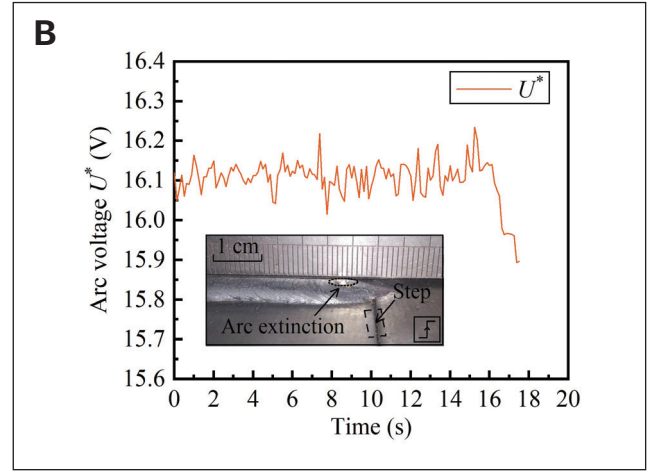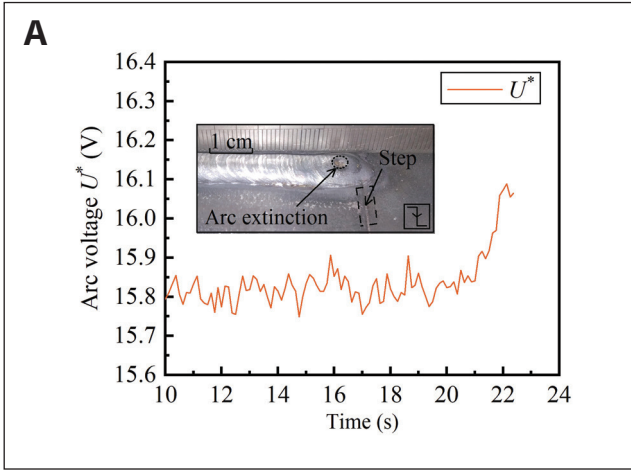
Fig. 7 — The obtained arc voltage U*: A — Experiment B1; B — Experiment B2.

to indirectly ensure the stability of the arc length. In this way, if the height of the welding torch was considered to be constant, the stability of the arc length indicated that the height of the weld surface was stable. Additionally, specifying different reference values of arc voltage obtained different weld surface heights (a larger reference value corresponded to a lower weld surface height).

Figure 10 presents the time response of U^* to the positive and negative step changes in v_f between 150 and 250 cm · min^{-1}, when the welding current and speed were 180 A and 8 cm · min^{-1}, respectively. It was seen from the change in U^* that the change in the weld pool surface caused by the adjustment of v_f could be detected by arc sensing. Additionally, the First Order Plus Dead Time model was used to identify the step response, and its transfer function is expressed as follows:

$$G(s) = \frac{K_p}{T_p s + 1} e^{-\tau_p s} \qquad (3)$$

where K_p, T_p, and τ_p represent the process gain, time constant, and dead time, respectively. The identified values of $[K_p, T_p, \tau_p]$ in the positive and negative step experiments were [−0.0039, 1.8524, 0] and [−0.0045, 2.8193, 0], respectively, and the model output curve had a good approximation to the original data, as shown in Fig. 10. It can be seen that the response of U^* to the step change in v_f was actually a simple first-order process without time delay. An intuitive cognition could then be obtained (i.e., a conventional controller can be used to demonstrate the practicability of U^* and meet the requirements of the control strategy instead of designing a complex model and controller, which needs to determine more model parameters). From this point of view, a proportional-integral-derivative (PID) controller was employed in this work.

Fuzzy Controller Design

In this work, the characteristic signal f_{mt} was chosen as the controlled variable to control the metal transfer stability of wire-filled GTAW by adjusting the wire feed speed in real
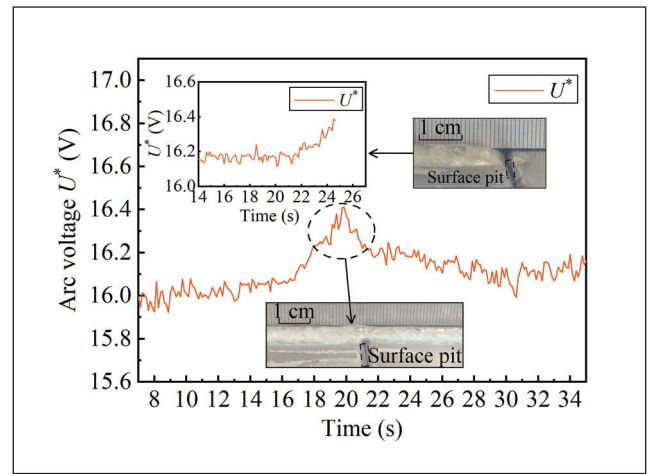

Fig. 8 — Arc voltage U* obtained in Experiment B3.

time. A Mamdani-type (Ref. 30) double-input single-output fuzzy controller was designed. To ensure the metal transfer stability, f_{mt} was expected to be controlled to zero. If e is the deviation between the actual value and the expected f_{mt}, and ce is the deviation change, then e and ce at an instant t can be expressed as follows:

$$e(t) = f_{mt}(t) \qquad (4)$$

$$ce(t) = e(t) - e(t-1) \qquad (5)$$

where e and ce were used as controller inputs and later fuzzified into fuzzy linguistic variables E and CE, respectively. The controller output (CV) was the increment of wire feed speed, and its fuzzy linguistic variable was denoted as CV. The universe of discourse for linguistic variables E, CE, and CV was [0, 6], [−6, 6], and [−2, 6], respectively. These fuzzy linguistic variables were described by the following fuzzy linguistic terms: positive large in size (PL), positive medium in size (PM), positive small in size (PS), zero (Z), negative small in size (NS), and negative large in size (NL). The linguistic

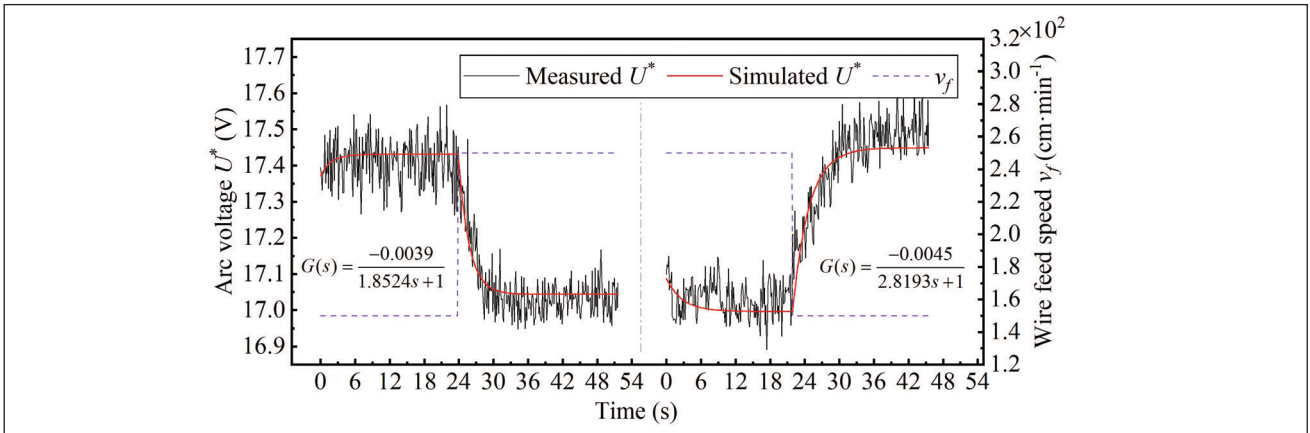Fig. 9 — The longitudinal weld section in Experiment B3.

Fig. 10 — The responses of arc voltage U* to the step changes in wire feed speed v$_f$ during bead-on-plate welding.

terms of each fuzzy linguistic variable were quantified by the membership function, as shown in Fig. 11.

The fuzzy control rules were determined by the hypothetical reasoning method. A typical fuzzy rule has the following form:

If E is A and CE is B, then CV is C.

where A, B, and C represent fuzzy sets. When the metal transfer was already in the uninterrupted bridging transfer mode, on one hand, the further increase in v$_f$ only caused the welding wire to continue to be fed into the weld pool without causing the change in f$_{mt}$, and, on the other hand, a too-high wire feed speed made the welding wire unable to melt in time due to insufficient heat and resulted in an unstable welding process.

In view of this, empirical fuzzy rules were formulated as shown in Table 2. Based on these rules, if the input is far from zero, a CV of PL will be output, and if both inputs are near zero, a CV of NS will be output. In this way, when the uninterrupted bridging transfer has been realized, the controller will slowly reduce v$_f$ to find the critical state between the uninterrupted and interrupted bridging transfer so that the welding wire will not be stuck on the workpiece due to the overly high v$_f$. It should be noted that although such a slow reduction of v$_f$ is not conducive to the maintenance of the uninterrupted bridging transfer, the short-time absence of liquid bridge during this critical state will not greatly affect the welding process. Finally, CV was obtained by fuzzy inference, and defuzzification was implemented by the centroid method.

PID Controller Design

A discrete incremental PID controller was designed to control the weld surface height. U^* was chosen as the controlled variable, and v_f was chosen as the control variable. U^* calculated according to Equation 2 at instant t and $U^*(t-1)$ obtained at instant $(t-1)$ were averaged with weights of 0.8 and 0.2, respectively, to obtain $U^*(t)$ at instant t. The reference voltage was denoted as U_r, which represents the voltage that U^* was expected to reach during feedback control. Error e_c at instant t can be obtained as follows:

$$e_c(t) = U_r(t) - U^*(t) \qquad (6)$$

The incremental form of the PID controller can be expressed as follows:

$$\Delta u(t) = K_p x_{c1}(t) + K_i x_{c2}(t) + K_d x_{c3}(t) \qquad (7)$$

where Δu was the increment of v_f, and K_p, K_i, and K_d were the adjustment parameters of the PID controller. x_{c1}, x_{c2}, and x_{c3} can be calculated by Equation 8:

$$\begin{cases} x_{c1}(t) = e_c(t) - e_c(t-1) \\ x_{c2}(t) = e_c(t) \\ x_{c3}(t) = e_c(t) - 2e_c(t-1) + e_c(t-2) \end{cases} \qquad (8)$$

It is easy for the integral accumulation to cause an overshoot, so when the error is too large, the proportional
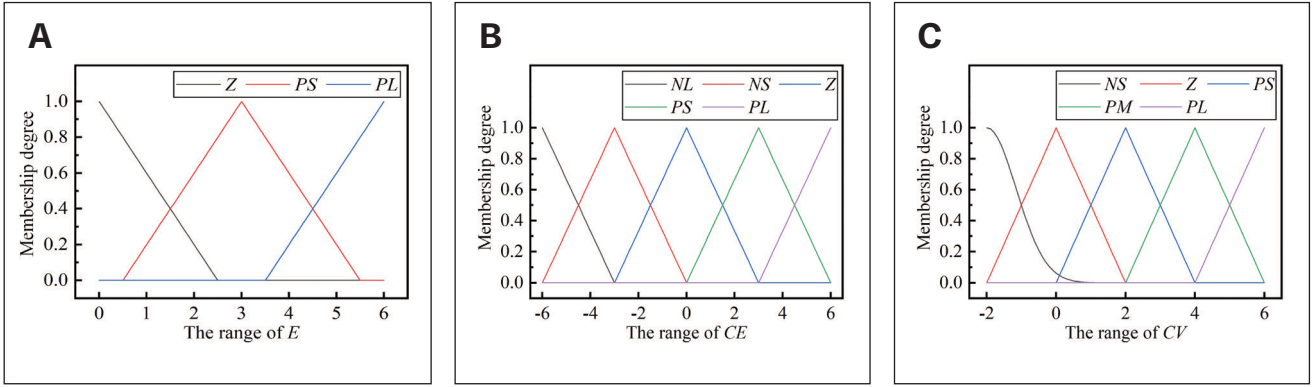
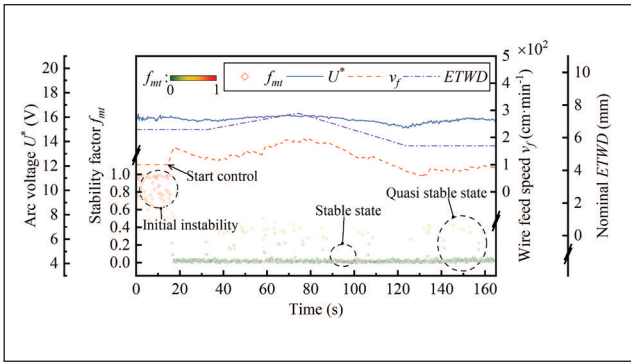Fig. 11 — Membership function plots: A — E; B — CE; C — CV.

Fig. 12 — The fuzzy control result of metal transfer in Experiment C1.

derivative (PD) control is employed to achieve integral separation as follows:

$$\Delta u(t) = -120x_{c1}(t) + 30x_{c3}(t), |x_{c2}(t)| > 0.45 \qquad (9)$$

During the actual process, the local small fluctuation in U^* was prone to making the controller misjudge the real change trend of U^*. For this reason, before performing PD control, it was necessary to judge the change trend of U^* so that the controller could always output the adjustment that reduces the error. Thus, if the error entered the range for the PD control at instant t, the sample data $[(x_1, U^*(t - n + 1)), (x_2, U^*(t - n + 2)), ..., (x_{n-1}, U^*(t - 1)), (x_n, U^*(t))]$ (x_n equals n) was extracted, and the least square estimation (denoted as k_1) of the first-order term coefficient of the univariate linear regression model of this data was calculated by Equations 10 and 11:

$$\overline{x} = (\textstyle\sum_{i=1}^{n} x_i)/n, \ \overline{U^*} = [\textstyle\sum_{i=1}^{n} U^*(t - n + i)]/n \qquad (10)$$

$$k_1(t) = \left[\textstyle\sum_{i=1}^{n} x_i U^*(t - n + i) - n\overline{x}\,\overline{U^*}\right] / (\textstyle\sum_{i=1}^{n} x_i^2 - n\overline{x}^2) \qquad (11)$$

where n was 6. If $k_1(t)$ was greater than 0.0089, it was considered that U^* was on the rise, and at that moment, a positive

Δu was desired. Then, if the Δu calculated by Equation 9 was negative at instant t, a positive Δu at the recent instant was taken as $\Delta u(t)$. Conversely, if $k_1(t)$ was less than −0.0089, a recent negative Δu was taken as $\Delta u(t)$.

When the error was small, the integral term was introduced and the segmented PID control was employed:

$$\begin{cases} \Delta u(t) = -73x_{c1}(t) - 16x_{c2}(t) - 3x_{c3}(t), \ 0.30 < |x_{c2}| \leq 0.45 \\ \Delta u(t) = -65x_{c1}(t) - 18x_{c2}(t) - 3x_{c3}(t), \ 0.15 < |x_{c2}| \leq 0.30 \\ \Delta u(t) = -45x_{c1}(t) - 19x_{c2}(t) - 3x_{c3}(t), \ \ \ \ 0 < |x_{c2}| \leq 0.15 \end{cases} \qquad (12)$$

Ultimately, Equations 9 and 12 constituted the control law of U^*.

Control Results

Experiments C1 and C2 were conducted to verify the effectiveness of the fuzzy controller. The control interval was 0.5 s, and the input scaling gain was 6. If the output was positive, the output scaling gain was 3, and if the output was negative, the output scaling gain was 2.5.

The control result of Experiment C1 is shown in Fig. 12. After starting the control, v_f first increased to make the unstable metal transfer quickly enter the uninterrupted bridging transfer mode and then decreased to find the critical state between the uninterrupted and interrupted bridging transfer. When the ETWD gradually increased and the metal transfer stability was weakened, v_f gradually increased, and then with the decrease in the ETWD, v_f decreased reasonably again and finally tended to be relatively flat. Throughout the whole process, most of the f_{mt} were distributed around zero, and a few were scattered outside of zero. The controller was able to ensure that the metal transfer was in a stable or quasi-stable state with the gradual change in the ETWD, although the fuzzy rule table did not include the equilibrium point at which the output was zero.

Figure 13 shows the experimental results under different output scaling gains when the output was negative in Experiment C2, where the step change in the ETWD caused the instability of metal transfer. Due to the controller action, it was seen that the initial instability and the instability caused by the positive step of the ETWD can be effectively suppressed under the adjustment of v_f. After the ETWD had a negative
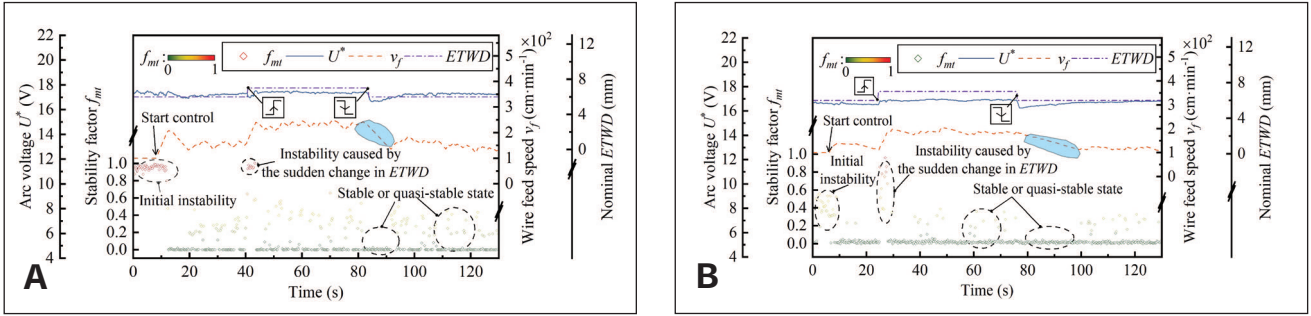
Fig. 13 — Fuzzy control results of metal transfer in Experiment C2: A — The output scaling gain of negative output is 2.5; B — the output scaling gain of negative output is 2.
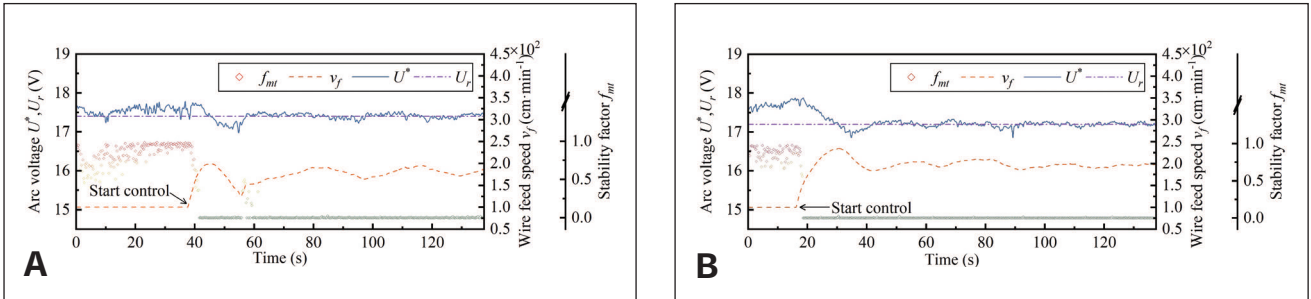

Fig. 14 — Control results of arc voltage: A — Experiment D1 (U_r is 17.4 V); B — Experiment D2 (U_r is 17.2 V).
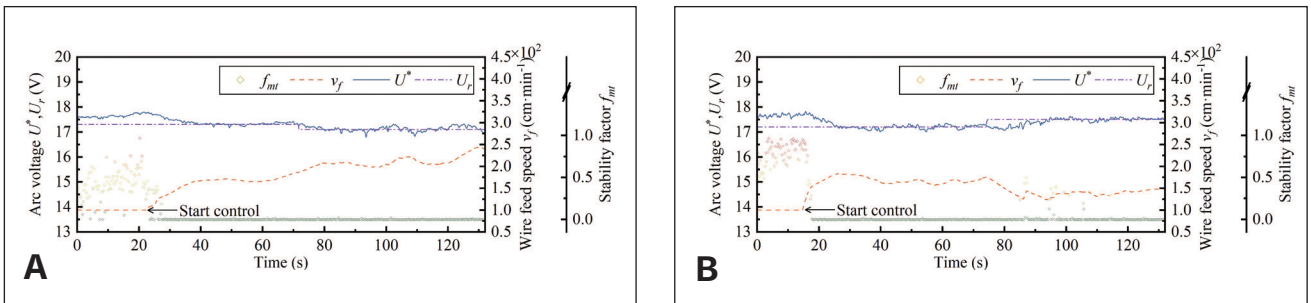

Fig. 15 — Control results of arc voltage: A — Experiment D3 (negative step of U_r from 17.3 to 17.1 V); B — Experiment D4 (positive step of U_r from 17.2 to 17.5 V).

step, v_f immediately decreased to find the critical state of metal transfer, and different output scaling gains affected the time to find this state.

Control of U^* was conducted in Experiments D1 to D4 and E1 to E2. It can be seen from Equation 2 that U^* was obtained by the average of $U_{g'}$ collected in the sampling window, so more samples of $U_{g'}$ in one sampling window were expected to be collected, allowing U^* to more accurately characterize the change in arc length. Meanwhile, it should be noted that if the liquid bridge existed for a shorter time, the sample number of $U_{g'}$ collected in a sampling window of length N was smaller (i.e., the value of $N – k$ was smaller). In view of this, the PID control can be enabled when the value of f_{mt} is small. Thus, in each control interval for Experiments D1 to D4 and E1 to E2, if f_{mt} was greater than 0.4, fuzzy control of the metal transfer stability was implemented; otherwise, PID control was implemented.

Since the control of the weld surface height was realized by indirectly controlling the arc voltage, the effectiveness of

the controller on the arc voltage control was verified first. As presented in Fig. 14, after introducing the closed-loop control, while the metal transfer remained relatively stable, the arc voltage U^* was also maintained around different U_r. It can be seen from Fig. 15 that even if U_r had a step change in the control process, the controller could still have a corresponding response to make U^* change toward a new reference voltage over a period of time, which also shows that this is an inertial process.

The control results for the weld surface height are shown in Figs. 16 and 17. In these two experiments, a step and a pit were preset on the workpiece surface, respectively. As shown in Figs. 16A and 17A, after starting control, U^* and v_f fluctuated relatively steadily, and the subsequent surface step or pit made U^* rise to a peak, which made v_f have a large adjustment so that U^* could change toward the reference value as much as possible and ensure the arc length stability. The mean absolute error (MAE) and the root mean square error (RMSE) were calculated to describe the overall perfor-
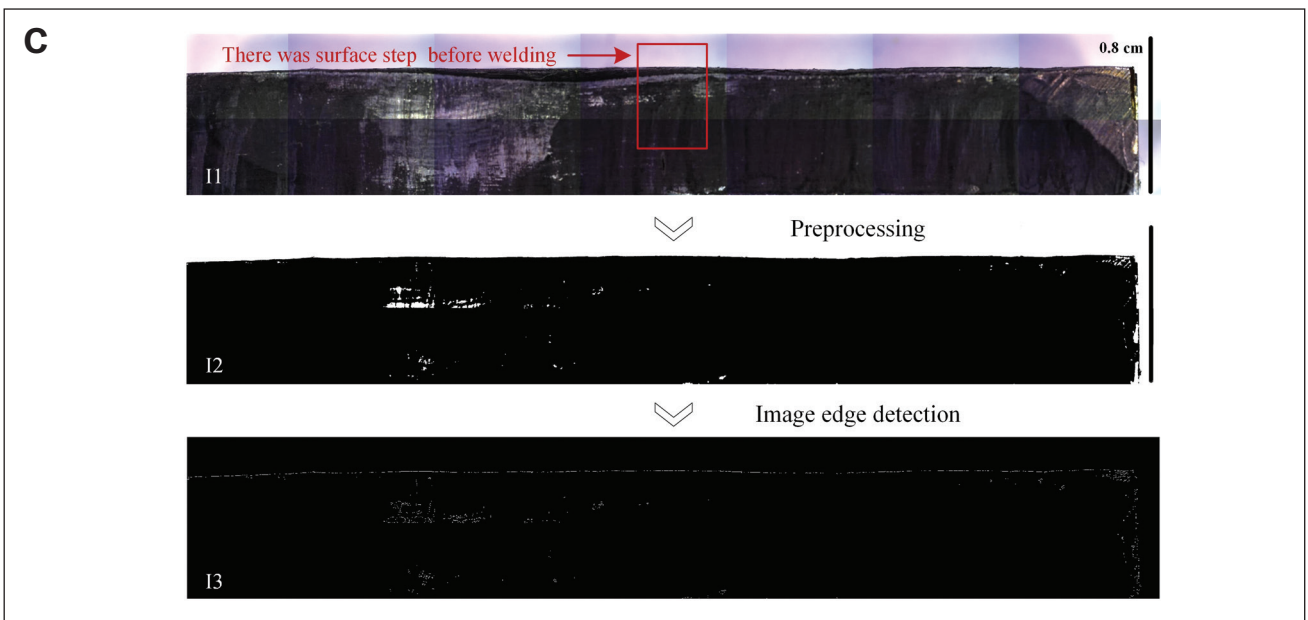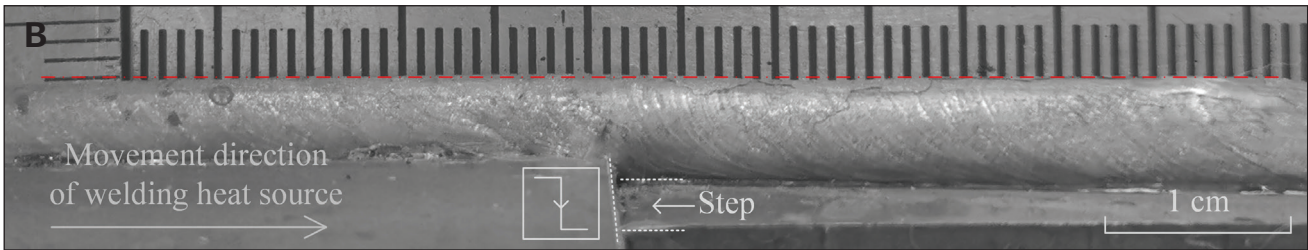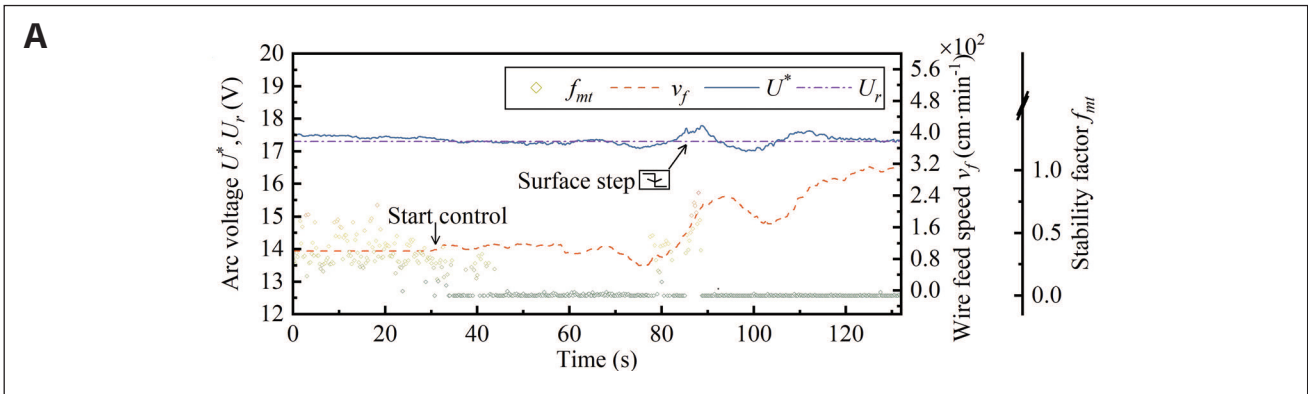
Fig. 16 — Control result of the weld surface height in Experiment E1: A — Experimental data; B — weld macromorphology; C — weld longitudinal section under a stereoscopic microscope or after image processing.

mance of the controller for U^*, as shown in Table 3. Figures 16B and 17B, respectively, show the macroscopic morphology of the weld surface, including the area of step and pit. It can be intuitively observed that even if there was a step or pit on the workpiece surface before welding, the height of the weld surface can still be relatively stable.

To further observe the weld surface height, the longitudinal section of the weld bead, including the step and pit areas, was cut by an electrical discharge machine, and the images of different areas of the longitudinal section were taken by a stereoscopic microscope, and then these images were stitched together to obtain the longitudinal section of the

weld bead, as shown in images I1 in Figs. 16C and 17C. It can be directly observed from the longitudinal section that the surface area where there was originally a step or pit became flat, and the entire weld surface height was relatively continuous. This is because the step or pit caused the change in U^*, and the controller adjusted v_f according to the deviation between U^* and its reference value U_r to change the weld pool height, thus indirectly ensuring the stability of the weld surface height after solidification (given the condition that the height of the welding torch was nominally stable). In the image I1 in Fig. 17C, the height of the surface area in front of
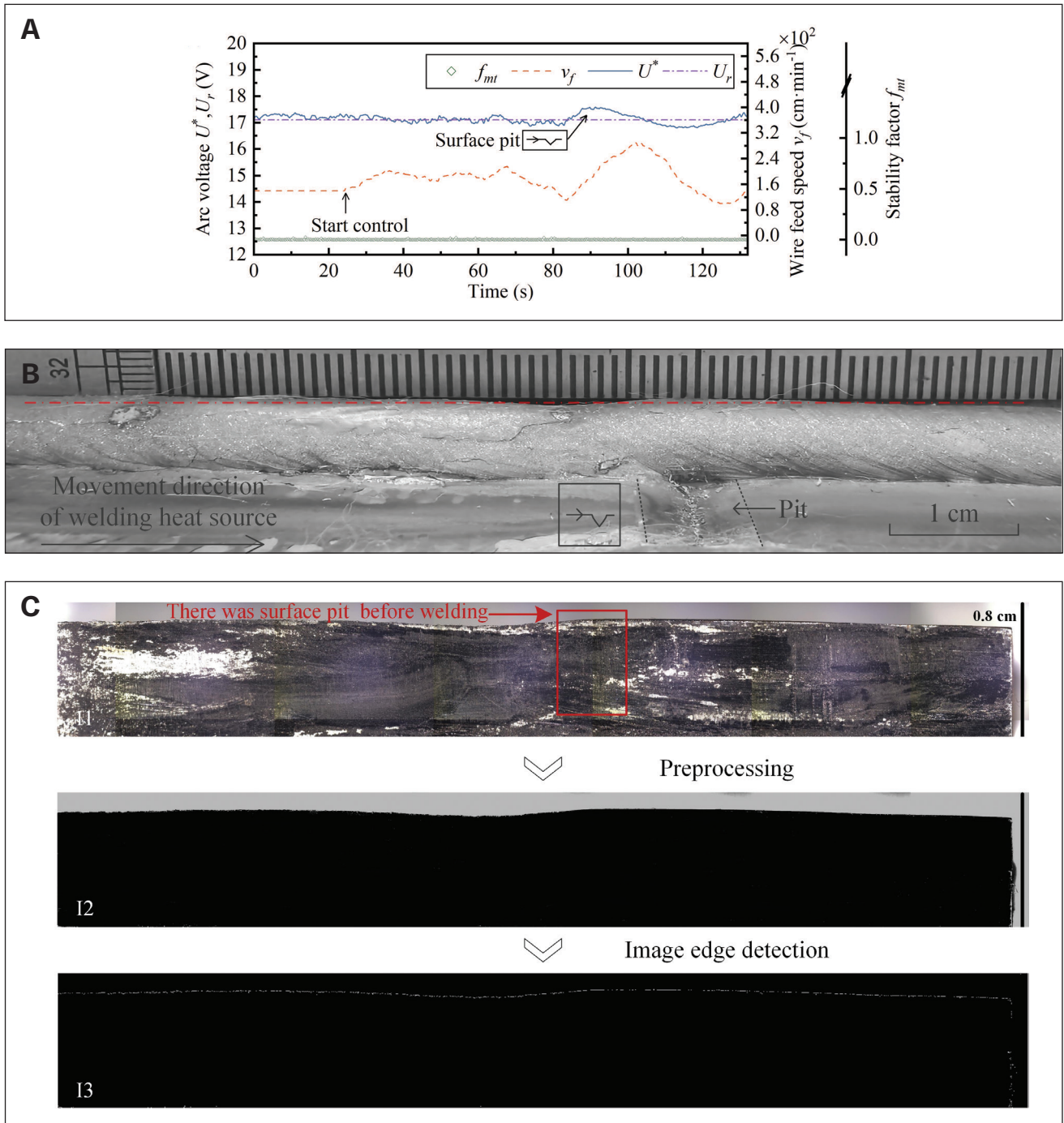
Fig. 17 — Control result of the weld surface height in Experiment E2: A — Experimental data; B — weld macromorphology; C — weld longitudinal section under a stereoscopic microscope or after image processing.

the pit slightly decreased, which was similar to the result of Experiment B3 shown in Fig. 9.

However, compared with the latter, the decreasing trend for the weld surface height near the pit was effectively suppressed by real-time control. Additionally, to quantify the weld surface height, image processing was performed on the longitudinal section of the weld. The original images were preprocessed and binarized to enhance the weld surface contour (as shown in the images I2 in Figs. 16C and 17C). The weld surface contours were then extracted using the

Sobel operator of edge detection (as shown in the images I3 in Figs. 16C and 17C).

Based on the scale bar and the pixel coordinates of the weld surface contours, the weld surface height can be estimated. The notion of weld surface height (denoted as H) in these two experiments is schematically shown in Fig. 18. Although the cutting trajectory, image shooting, and stitching process will produce errors on the estimated value of H, the estimation results in this work can still be considered reliable. It can be seen from the longitudinal distribution of the estimated weld
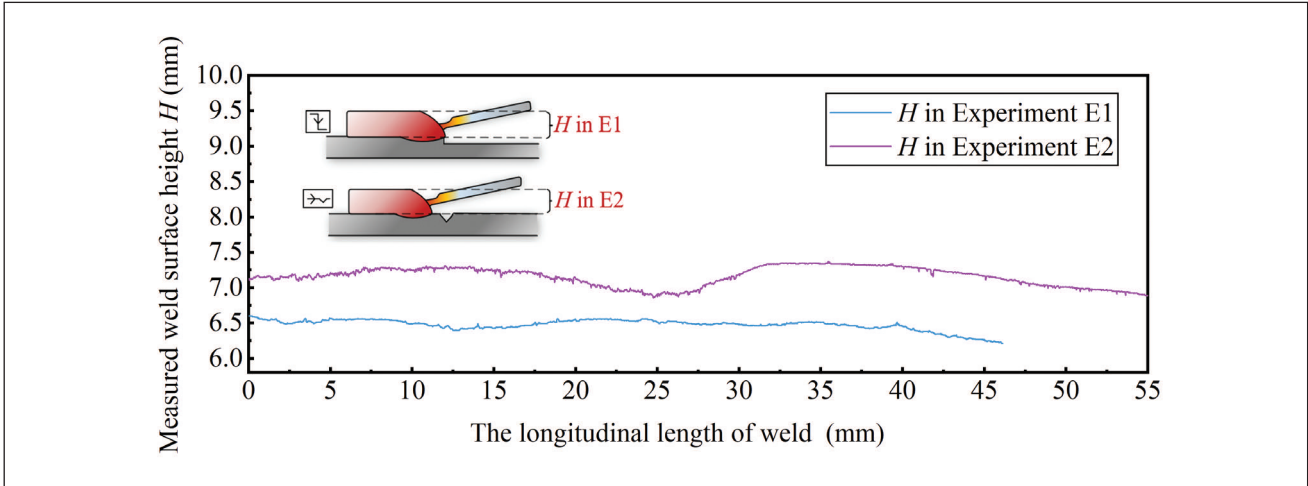
Fig. 18 — The measured weld surface heights of Experiments E1 and E2 extracted based on digital image processing.

Table 3 — The MAE and RMSE for PID Control of Arc Voltage or Weld Surface Height (in V)

Experiment No.	D1	D2	D3	D4	E1	E2
$MAE = \frac{1}{n}\sum_{i=1}^{n}\lvert U^*(i) - U_r(i)\rvert$	0.0529	0.0488	0.0696	0.0842	0.1070	0.1380
$RSME = \left[\frac{1}{n}\sum_{i=1}^{n}\lvert U^*(i) - U_r(i)\rvert^2\right]^{1/2}$	0.0649	0.0635	0.0932	0.1244	0.1481	0.1765

surface height in Fig. 18 that the weld surface near the original step or pit area was relatively flat, which demonstrated that the strategy of controlling the arc voltage U^* by adjusting the wire feed speed v_f can indirectly ensure the stability of the weld surface height.

Conclusions

In this work, a global and local arc sensing method that collects both global and local arc information was proposed. This method can be used to monitor metal transfer during wire-filled GTAW. Under the interference of metal transfer, it can also be used to monitor the weld surface height by sensing the change in arc length. Based on the extracted characteristic signals, namely the stability factor f_{mt} for metal transfer and the average global arc voltage in the presence of the liquid bridge U^*, a series of preliminary feedback control experiments of process stability were conducted. They verified the effectiveness and potential of the proposed method. The following main conclusions can be drawn:

1) The presence or absence of a liquid bridge can be clearly distinguished by local arc sensing, and f_{mt} can be used to characterize the metal transfer stability. The closer f_{mt} is to zero, the more stable the metal transfer.

2) Based on the global and local arc sensing, U^* can be extracted by decoupling the dynamic interference signals of metal transfer to better characterize the change in arc length or the weld surface height under the interference of metal transfer.

3) A fuzzy controller and PID controller were designed to control the metal transfer stability and weld surface height. The results showed that, with the feedback control, the metal transfer can be controlled to a stable or quasistable state, and the consistency of the weld surface height can be guaranteed even when the workpiece surface height changes.

In this work, the preliminary control practice was relatively simple, but it shows the potential of the proposed arc sensing method. In a future study, the relevant strategies will be further improved to better handle practical problems.

References

1. Zhang, Y. M., Wang, Q. Y., and Liu, Y. K. 2021. Adaptive intelligent welding manufacturing. *Welding Journal* 100(1): 63-s to 83-s. DOI: 10.29391/2021.100.006

2. Xiong, J., Pi, Y. P., and Chen, H. 2019. Deposition height detection and feature point extraction in robotic GTA-based additive manufacturing using passive vision sensing. *Robotics and Computer Integrated Manufacturing* 59: 326–334. DOI: 10.1016/j.rcim.2019.05.006

3. Xiong, J., Liu, G. C., and Pi, Y. P. 2019. Increasing stability in robotic GTA-based additive manufacturing through optical measurement and feedback control. *Robotics and Computer Integrated Manufacturing* 59: 385–393. DOI: 10.1016/j.rcim.2019.05.012

4. Xiong, J., Zhang, Y. Y., and Pi, Y. P. 2020. Control of deposition height in WAAM using visual inspection of previous and current layers. *Journal of Intelligent Manufacturing* 32: 2209–2217. DOI: 10.1007/s10845-020-01634-6

5. Zhao, D. B., Chen, S. B., and Wu, L. 1999. Surface height and geometry parameters for describing shape of weld pool during pulsed GTAW. *SPIE Proceedings Series* 3833: 91–98.

6. Chen, Z. Y., Chen, J., and Feng, Z. L. 2017. Monitoring weld pool surface and penetration using reversed electrode images. *Welding Journal* 96(10): 367-s to 375-s.

7. Saeed, G., and Zhang, Y. M. 2007. Weld pool surface depth measurement using a calibrated camera and structured light. *Measurement Science and Technology* 18(8): 2570–2578. DOI: 10.1088/0957-0233/18/8/033

8. Li, C. K., Shi, Y., Gu, Y. F., and Yuan, P. 2018. Monitoring weld pool oscillation using reflected laser pattern in gas tungsten arc welding. *Journal of Materials Processing Technology* 255: 876–885. DOI: 10.1016/j.jmatprotec.2018.01.037

9. Song, H. S., and Zhang, Y. M. 2007. Three-dimensional reconstruction of specular surface for a gas tungsten arc weld pool. *Measurement Science and Technology* 18(12): 3751–3767. DOI: 10.1088/0957-0233/18/12/010

10. Song, H. S., and Zhang, Y. M. 2008. Measurement and analysis of three-dimensional specular gas tungsten arc weld pool surface. *Welding Journal* 87(4): 85-s to 95-s.

11. Song, H., and Zhang, Y. M. 2009. Error analysis of a three-dimensional GTA weld pool surface measurement system. *Welding Journal* 88(7): 141-s to 148-s.

12. Zhang, W. J., Wang, X. W., and Zhang, Y. M. 2013. Analytical real-time measurement of a three-dimensional weld pool surface. *Measurement Science and Technology* 24(11): 115011. DOI: 10.1088/0957-0233/24/11/115011

13. Zhang, W., Liu, Y. K., Wang, X., and Zhang, Y. M. 2012. Characterization of three-dimensional weld pool surface in GTAW. *Welding Journal* 91(7): 195-s to 203-s.

14. Liu, Y. K., and Zhang, Y. M. 2014. Model-based predictive control of weld penetration in gas tungsten arc welding. *IEEE Transactions on Control Systems Technology* 22(3): 955–966. DOI: 10.1109/TCST.2013.2266662

15. Liu, Y. K., and Zhang, Y. M. 2013. Control of 3D weld pool surface. *Control Engineering Practice* 21(11): 1469–1480. DOI: 10.1016/j.conengprac.2013.06.019

16. Liu, Y. K., Zhang, W. J., and Zhang, Y. M. 2015. Dynamic neuro-fuzzy-based human intelligence modeling and control in GTAW. *IEEE Transactions on Automation Science and Engineering* 12(1): 324–335. DOI: 10.1109/TASE.2013.2279157

17. Lv, N., Xu, Y. L., Zhang, Z. F., Wang, J. F., Chen, B., and Chen, S. B. 2013. Audio sensing and modeling of arc dynamic characteristic during pulsed Al alloy GTAW process. *Sensor Review* 33(2): 141–156. DOI: 10.1108/02602281311299680

18. Lv, N., Zhong, J. Y., Chen, H. B., Lin, T., and Chen, S. B. 2014. Real-time control of welding penetration during robotic GTAW dynamical process by audio sensing of arc length. *The International Journal of Advanced Manufacturing Technology* 74: 235–249. DOI: 10.1007/s00170-014-5875-7

19. Chen, C., Xiao, R. Q., Chen, H. B., Lv, N., and Chen, S. B. 2020. Arc sound model for pulsed GTAW and recognition of different penetration states. *The International Journal of Advanced Manufacturing Technology* 108(9–10): 3175-3191. DOI: 10.1007/s00170-020-05462-z

20. Li, P. J., and Zhang, Y. M. 2001. Precision sensing of arc length in GTAW based on arc light spectrum. *Journal of Manufacturing Science and Engineering* 123(1): 62–65. DOI: 10.1115/1.1349719

21. Yu, H. W., Song, J. Q., Zhang, G. A., Pu, J. Z., Chen, H. B., and Chen, S. B. 2015. The effects of arc length on welding arc characteristics in Al–Mg alloy pulsed gas tungsten arc welding. *Robotic Welding, Intelligence and Automation*: 321–335. DOI: 10.1007/978-3-319-18997-0_28

22. Cook, G. E. 1983. Robotic arc welding: Research in sensory feedback control. *IEEE Transactions on Industrial Electronics* 30(3): 252–268. DOI: 10.1109/TIE.1983.356736

23. Wang, Q. L., Yang, C. L., and Geng, Z. 1993. Separately excited resonance phenomenon of the weld pool and its application. *Welding Journal* 72(9): 455-s to 462-s.

24. Li, X. R., Shao, Z., Zhang, Y. M., and Kvidahl, L. 2013. Monitoring and control of penetration in GTAW and pipe welding. *Welding Journal* 92(6): 190-s to 196-s.

25. Koseeyaporn, P., Cook, G. E., and Strauss, A. M. 2000. Adaptive voltage control in fusion arc welding. *IEEE Transactions on Industry Applications* 36(5): 1300–1307. DOI: 10.1109/28.871278

26. Crawford, R., Cook, G. E., Strauss, A. M., and Hartman, D. A. 2006. Adaptive voltage control of gas tungsten arc welding. *International Journal of Modelling, Identification and Control* 1(2): 133–139. DOI: 10.1109/28.871278

27. Wang, H., Lei, T., Rong, Y. M., Shao, W. J., and Huang, Y. 2020. Arc length stable method of GTAW based on adaptive Kalman filter. *Journal of Manufacturing Processes* 63: 130–138. DOI: 10.1016/j.jmapro.2020.01.029

28. Zou, S. Y., Wang, Z. J., Hu, S. S., Zhao, G. C., and Chen, Y. Q. 2020. Effects of filler wire intervention on gas tungsten arc: Part I — Mechanism. *Welding Journal* 99(9): 246-s to 254-s. DOI: 10.29391/2020.99.023

29. Zou, S. Y., Wang, Z. J., Hu, S. S., Zhao, G. C., and Chen, Y. Q. 2020. Effects of filler wire intervention on gas tungsten arc: Part II — Dynamic behaviors of liquid droplets. *Welding Journal* 99(10): 271-s to 279-s. DOI: 10.29391/2020.99.025

30. Mamdani, E. H., and Assilian, S. 1975. An experiment in linguistic synthesis with a fuzzy logic controller. *International Journal of Man-Machine Studies* 7(1): 1–13. DOI: 10.1006/ijhc.1973.0303

SHUANGYANG ZOU, ZHIJIANG WANG (*wangzj@tju.edu.cn*), **YUE CAO**, and **SHENGSUN HU** are with the Tianjin Key Laboratory of Advanced Joining Technology, School of Materials Science and Engineering, Tianjin University, Tianjin, China.